Vacuum 183 (2021) 109820

Contents lists available at ScienceDirect

Vacuum

journal homepage: http://www.elsevier.com/locate/vacuum

Microstructure and mechanical properties of borided $CoCrFeNiAl_{0.25}Ti_{0.5}$ high entropy alloy produced by powder metallurgy

Azmi Erdogan [a,*], Ali Günen [b], Mustafa Sabri Gök [c], Sakin Zeytin [d]

[a] Department of Metallurgy and Materials Engineering, Faculty of Engineering, Architecture and Design, Bartın University, Bartın, Turkey
[b] Department of Metallurgy and Materials Engineering, Faculty of Engineering and Natural Sciences, Iskenderun Technical University, Hatay, Turkey
[c] Department of Mechanical Engineering, Faculty of Engineering, Architecture and Design, Bartın University, Bartın, Turkey
[d] Department of Metallurgy and Materials Engineering, Faculty of Engineering, Sakarya University, Sakarya, Turkey

ARTICLE INFO

Keywords:
High entropy alloy
Boriding
$CoCrFeNiAl_{0.25}Ti_{0.5}$
Mechanical properties
Fracture toughness
Powder metallurgy

ABSTRACT

$CoCrFeNiAl_{0.25}Ti_{0.5}$ high entropy alloy alloys (HEA), produced by powder metallurgy were subjected to boriding to improve their mechanical properties. Sintering was carried out at 1200 °C for 2 h in Ar, and boriding was performed at 900, 1000 and 1100 °C for 2 h using a 90 wt% B_4C + 10 wt% $NaBF_4$ boriding powder mixture. Microstructures, densities, surface roughnesses, and mechanical properties (hardness, fracture toughness and nanoindentation responses) of the samples were investigated. FCC, BCC and sigma phases had been observed after sintering, whereas complex metal borides were formed on the surfaces after boriding. Relative density values were between 85% and 90%. Significant increases in surface hardness were observed after boriding due to formation of hard, silicide-free boride layers. The boride layer thickness and hardness increased with increasing boriding temperature. The elastic modulus of the surface of the sintered sample (47.07 GPa) increased with the boriding process to values in the range of 140–151 GPa. Fracture toughness values between 3.57 and 4.25 MPa $m^{1/2}$ were obtained in borided samples, and increasing the boriding temperature reduced the fracture toughness.

1. Introduction

High entropy alloys (HEA), are multicomponent solid solutions that are being studied extensively for the many properties they can be tailored to possess (high strength, high temperature stability, high wear and corrosion resistance) that cannot be otherwise achieved simultaneously in traditional alloys [1,2]. Unlike traditional alloys which are built on a single element, these alloys contain at least 5 or more principal elements in equimolar or close to equimolar ratios [3,4]. There can be many types of classifications for these alloys as well as classification according to their entropy values. Generally, alloys containing one or two elements can be called “low entropy alloys”, alloys containing three or four elements “medium entropy alloys” and alloys containing more than five equimolar alloy elements can be called “high entropy alloys” [5]. High entropy alloys can exhibit properties such as high strength, good ductility, high oxidation and wear resistance thanks to the 4 core effect [6,7]. In the production of high entropy alloys, casting and powder metallurgy (P/M) methods are generally used.

P/M has some advantages in the manufacturing of final products. Much less finishing is required, and this is important for achieving low cost and reducing environmental pollution [8,9]. In addition, powder metallurgy offers advantages such as production repeatability, dimensional accuracy and good surface quality [10,11]. Production by powder metallurgy is particularly advantageous for high entropy alloys containing components with very different properties. Because the elements show very different melting temperatures and density values compared to each other, many problems can arise during casting. However, since melting is not required for production with P/M, high-alloy materials with different melting temperatures and densities can be produced with relative ease [12]. P/M is also one of the most suitable methods for producing metallic components with dimensions closest to final. Today, P/M is used extensively in the manufacturing of many automotive parts and structural materials [13]. By changing the microstructure, materials with exceptionally high corrosion and wear resistance can be obtained [14]. However, the mechanical properties of the materials produced by P/M may be inferior to mechanical properties of the cast materials due to residual porosity in the structure after production [15].

Boriding is a thermo-chemical surface treatment that is used to obtain a hard and durable structure on the surface [16–18]. In addition to steels, nickel, cobalt, titanium and molybdenum alloys can also be

* Corresponding author.
E-mail address: aerdogan@bartin.edu.tr (A. Erdogan).

https://doi.org/10.1016/j.vacuum.2020.109820
Received 5 August 2020; Received in revised form 28 September 2020; Accepted 30 September 2020
Available online 6 October 2020

borided [19–21]. The high hardness, high wear resistance and low friction coefficient obtained on the surface by boriding enables borided parts to be used extensively in the industrial applications where wear and friction are a concern. Typical applications include die-casting molds, bearings, shafts, gears etc. [22–24].

Boron has been investigated as an alloying element in high entropy alloys. Hou et al. [25] investigated the effect of boron additions of up to $x = 0.2$ ratio on the microstructure and mechanical properties of AlFeCoNiBx alloy with the addition of boron. They observed the formation of two different FCC structures apart from the B2 phase in the microstructure. In addition, with the increase in the boron content, they detected increased yield strength, tensile strength and hardness values. In another study, Chang et al. [26] $FeCr_xCoNiB$ deposited a HEA on a AISI 1045 substrate by laser cladding. They stated that in the $FeCr_{0.5}$-CoNiB alloy, 860 H V hardness was obtained owing to the presence of boron. Although there are a few similar studies related to the use of boron in high entropy alloys, there are not many studies on its use as a coating. The only study on the boriding of HEAs is that of Lindner et al. [27], who borided CoCrFeMnNi and CoCrFeNi HEAs at 900 °C for 5 h using Ekabor II powders. The authors reported that boron causes the formation of interstitial solid solutions or precipitates in thermochemical surface treatments and that boriding results in complex coatings containing silicides and borides. They reported that the wear resistance of the HEAs increased due to the hardness increase associated with the formation of silicide and boride containing layers. However, in the literature it is stated that the formation of nickel silicides is inevitable if Si-containing boriding powders are used in the boriding of Ni-based alloys [28]. Nickel silicides formed have been notoriously characterized by a high degree of porosity and diminished hardness compared to borides [29–31]. As seen from the studies in the literature, the boriding of HEAs is a relatively new subject. The current study is therefore focused on the boriding of HEAs produced from powder metallurgy and on the effect of the applied boriding process on the microstructure, hardness, fracture toughness and elastic modulus of HEAs.

2. Experimental

High purity and Al, Co, Cr, Fe, Ni and Ti powders, less than 45 μm (−325 mesh) in diameter, were commercially supplied from Alfa Aesar. The purities of the powders are 99.5% for Al, 99.8% for Co, 99% for Cr, 99.8% for Ni, 98% for Fe and 99.5% for Ti. The powders were prepared in the composition of $CoCrFeNiAl_{0.25}Ti_{0.5}$ and mixed under atmospheric conditions at 250 rpm for 4 h. The powder blend was then weighed and poured into a mold to produce samples of 15 mm diameter and 3 mm thickness. Cold compaction was carried out under 250 MPa load. The samples were then sintered at 1200 °C for 2 h in Ar. Then the samples were borided at temperatures of 900, 1000 and 1100 °C for 2 h in the boronizing environment (90 wt% B_4C + 10 wt% KBF_4) under Ar gas. The nomenclature used for the samples are provided in Table 1.

Density (ρ) measurements of P/M materials were carried out according to Archimedes' principle by measuring their weights in air and pure water:

$$\rho = \text{weight x density of fluid / (weight – apparent immersed weight)} \quad (1)$$

Surface roughness was measured using a Wave System Hommelwerke T8000 2D profilometer. The measurements were made at 1 mm/s speed along a 4 mm distance on each sample surface and reported as the average of 5 measurements.

After sintering and boriding, metallographic samples were prepared with a precision cutting device for SEM, EDS and XRD analysis. Subsequently, samples were subjected to grinding with 180, 240, and 2000 grit SiC papers and polishing with 1 μm Al_2O_3 paste. Etching of the samples was done with 2% Nital. Metallographic studies were carried out on the polished and etched sections of the samples using a Thermo Scientific Apreo S SEM equipped with an Ultra Dry EDS Detector. The thickness of the boride layer was determined by SEM and the phases formed on the surface of the P/M samples were verified by X-ray diffraction (XRD) using a computer-controlled Rigaku Smart LabTM diffractometer. Cu Kα radiation (λ = 0.154 nm); a 2θ angle range of 30°–90°, and step size of Δ2θ = 0.006° was used. Phase identifications were made by using PDXL software.

Microhardness measurements were performed in accordance with the ASTM E384 standard using a FM-700 Future-Tech hardness tester with a pyramid indenter, with 50 g load and 15 s standby time. Nanoindentation tests were performed with a Berkovich tip according to Oliver-Pharr analysis method with a Hysitron TI-950 TriboIndenter nanoindenter device [32]. Tests were done on a 1 × 5 analysis matrix under 10 μN peak load. Force-controlled loading was performed using a trapezoidal function. The load was increased at a constant loading speed in 30 s, held for 10 s, and then gradually released within 30 s.

A wide variety of formulas are used for determining the fracture toughnesses of coatings. Using the equation which is used in the measurement of fracture toughness of ceramic materials will give the most accurate result since the properties of the boride layers formed as a result of boriding of steels are similar to those of ceramics [33].

$$Kc = 0.016\ (E/Hv)^{1/2}\ (p/c^{3/2}) \quad (2)$$

Kc: Fracture toughness ($MPa.m^{1/2}$), E: Modulus of elasticity (kg/mm^2), Hv: Vickers hardness of the coating layer (kg/mm^2), p: Applied load (MN), c: Crack half-length (m).

3. Results and discussion

3.1. Density and surface roughness

The density and surface roughness values of $CoCrFeNiAl_{0.25}Ti_{0.5}$ alloy, cold compacted at 250 MPa and sintered in 1200 °C and borided using 90% B_4C + 10% KBF_4 powders are given in Table 2.

Table 2 shows that the relative density value of the sintered sample in the Ar environment is 85%. The relative density values increased only slightly with the boriding process after sintering. This can be attributed to boron diffusion towards the interior of the samples with the boriding process. The diffusion of boron and/or boron-containing compounds was effective in reducing some of the porosity that remained after sintering. Due to the fact that the boriding treatment was carried out at a temperature close to the sintering temperature, the boriding treatment served as a secondary sintering process, and additionally allowed boron atoms to diffuse towards the interior, forming solid solution(s) or borides with the substrate material. The presence of porosity also allowed boron to penetrate porous regions in the gaseous state in the form of molecular compounds such as BF_3 during the boriding process. As a

Table 1
Sample nomenclature and process parameters used in the boriding of $CoCrFeNiAl_{0.25}Ti_{0.5}$.

Sample	Sintering Parameters (under Ar)	Boriding Parameters (in 90 wt% B_4C + 10 wt% KBF_4 powder mixture under Ar)
S1	1200°C-2h	–
S2	1200°C-2h	900°C-2h
S3	1200°C-2h	1000°C-2h
S4	1200°C-2h	1100°C-2h

Table 2
Density and surface roughness values of samples after sintering and boriding.

Sample	Density (g/cm^3)	Relative density (%)	Surface roughness	
			Ra (μm)	Rz (μm)
S1	6.35	85.01	1.90	18.30
S2	6.50	87.48	3.80	35.20
S3	6.65	88.90	3.56	27.65
S4	6.72	90.01	2.95	28.46

result, the porosity and oxides in the microstructure decreased.

The lowest density was seen in sample S1 (6.35 g/cm^3), while the highest density was observed in sample S4 (6.72 g/cm^3). The relative densities of the samples range between 87% and 90%. The density values obtained in the samples were similar to the density values seen in the samples produced by powder metallurgy in the literature. Karwan-Baczewska [34] stated that by adding boron to Distaloy SA powders which were then cold pressed at 600 MPa and sintered 1200 °C for 1 h, the relative density values of the samples begin from 75% and can reach up to 94% depending on process parameters. In another study, Erdogan et al. [35] stated that AISI 1010 steel has density values between 5.90-6.20 and 21–29% porosity after borosintering.

When the samples are evaluated in terms of surface roughness, it is seen that all borided samples have higher Ra and Rz values. It is thought that this is due to the sintering of boronizing powders absorbed onto the surface during the boriding process. With the increase in the boriding process temperature, the boronizing powders penetrated further into the surface, so there was some decrease in surface roughness values. It has been observed in other studies that the roughness values generally tend to increase with the boriding process when it is applied to samples produced by P/M [35,36].

3.2. Microstructure characterization

An SEM image and complementary EDS analysis of the CoCrFeNiAl$_{0.25}$Ti$_{0.5}$ alloy subjected to sintering in Ar for 2 h at 1200 °C is given in Fig. 1. The SEM image clearly shows that a 10 μm-thick layer with high oxygen content (about 13.05 wt% O) has formed on the surface of the sintered sample. Beneath this layer is the substrate; however there are some oxides present in regions near the oxide/substrate interface. Moving further into the interior, the oxygen concentration decreases. This situation shows that oxygen originating from the trapped air between the powders spreads towards the surface during sintering. In the elemental distribution, the distribution seen in high entropy alloys with similar content was observed. Nickel and titanium, which have a high negative mixing enthalpy, were enriched in areas far from the surface. It was expected that the aluminum content would increase in this region, but the aluminum content was higher in the surface. One of the reasons for this is the high affinity of aluminum to oxygen. While Co has a homogeneous distribution as expected, it is likely that Fe and Cr will be in the same phase due to the close mixing enthalpy values.

In Fig. 2, SEM and EDS analyses of CoCrFeNiAl$_{0.25}$Ti$_{0.5}$ alloy, which were subjected to boriding process for 2 h at 900, 1000 and 1100 °C after 2 h of sintering in Ar at 1200 °C, are shown. It can be seen that a double-layer coating was obtained at all boriding temperatures. From these layers, it was seen that the layer on the surface was rougher and the below layer had a relatively more homogeneous appearance. With increasing boriding temperature, the roughness of the surface decreases due to enhanced boron diffusion, and the boride layer grows towards the interior.

In terms of morphology, the boride layer is continuous and no cracks are present on the surfaces of the borided samples. Similar to boride coatings formed on the surfaces of low alloy P/M steels [35,36], the boride layer is smooth and contains oxides. This can be attributed to the oxygen content in the air gaps that remained in between the powders during cold compaction. However, the presence of these air gaps also help the diffusion of the boron to the interior during boriding, enabling thicker (about 363 μm) boride layers to form compared to borided wrought steels [17–24]. Oxides in the coating layer are relatively fewer when compared to the interior. Oxide islets in the coating layer and in the inner regions are characteristic of samples produced from powder metallurgy and are not seen in the boride layers obtained in the boriding of wrought alloys. Hardness is a measure of a material's resistance to localized plastic deformation. Therefore, it is clear that porosity in the structure may impair certain mechanical properties such as hardness. This is the reason that the boride layers formed on P/M steels may have inferior mechanical properties (hardness, elasticity modulus) compared to boride layers formed on wrought steels. It is possible to produce steels

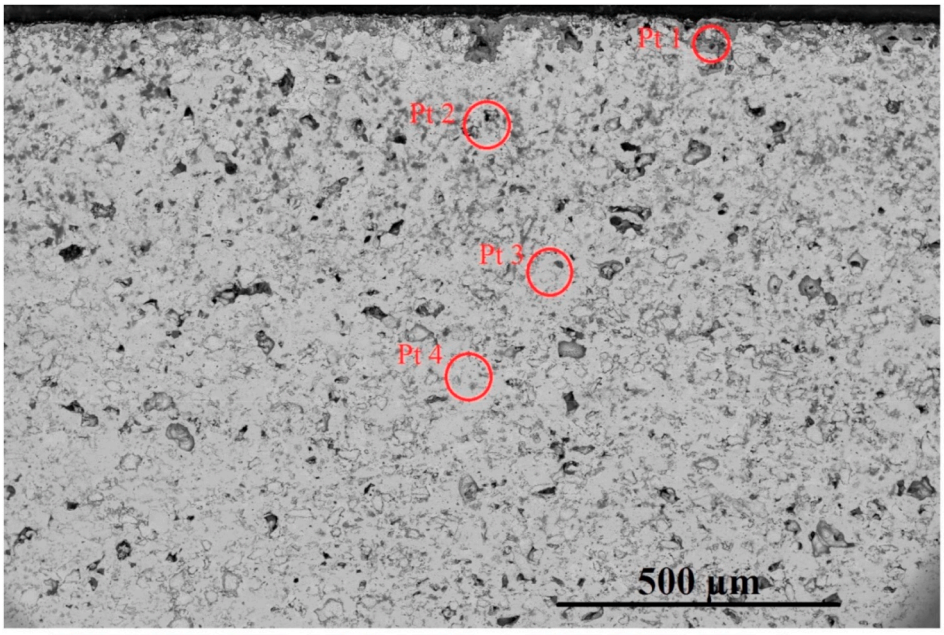

Wt.%	Fe-L	Cr-K	Co-L	Ni-L	Al-K	Ti-K	O-K
Pt1	18.73	22.54	17.87	16.76	5.33	5.72	13.05
Pt2	20.75	21.91	18.01	19.72	4.28	6.26	9.07
Pt3	21.56	19.54	17.64	21.47	3.71	8.56	7.52
Pt4	25.02	17.48	17.48	22.54	2.77	9.81	4.90

Fig. 1. SEM and EDS analysis of CoCrFeNiAl$_{0.25}$Ti$_{0.5}$ alloy, which was subjected to sintering in Ar environment for 2 h at 1200 °C.

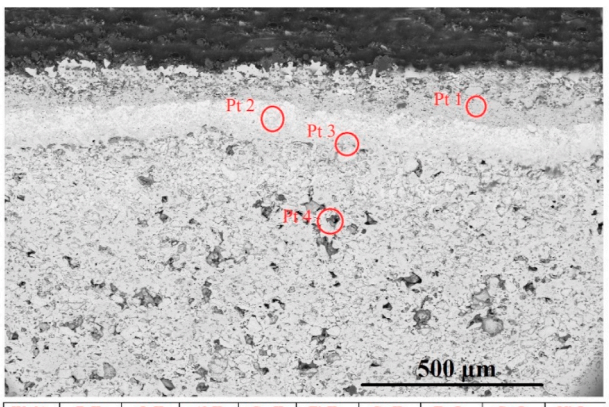

Wt.%	B-K	O-K	Al-K	Ca-K	Ti-K	Cr-K	Fe-L	Co-L	Ni-L
Pt1	9.22	8.20	8.95	1.25	6.29	11.52	15.72	14.75	24.10
Pt2	8.84	4.25	7.98	0.56	4.15	11.89	20.62	13.05	28.67
Pt3	8.27	4.40	4.35	1.00	3.91	11.62	23.87	15.73	26.86
Pt4	1.87	6.32	4.91	0.11	1.15	20.16	25.36	16.96	23.17

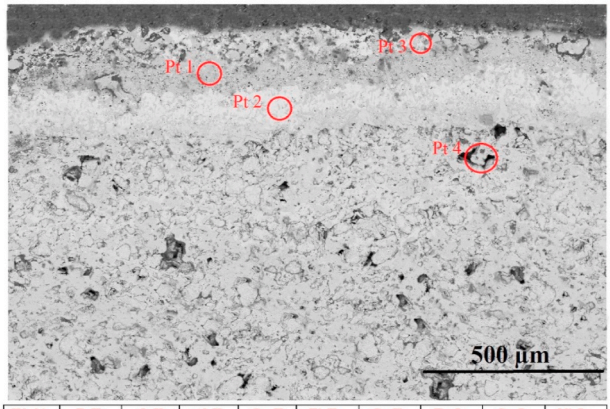

Wt.%	B-K	O-K	Al-K	Ca-K	Ti-K	Cr-K	Fe-L	Co-L	Ni-L
Pt1	10.78	9.52	3.15	2.52	11.01	23.10	16.42	14.05	9.45
Pt2	13.04	6.06	6.74	0.84	9.38	16.06	13.95	15.38	18.55
Pt3	8.31	4.65	3.11	0.72	2.56	15.34	26.26	14.91	24.13
Pt4	1.62	9.18	3.77	0.27	0.77	10.28	30.22	14.27	29.62

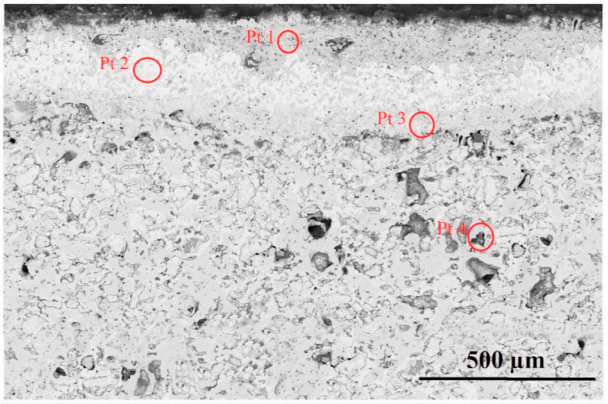

Wt.%	B-K	O-K	Al-K	Ca-K	Ti-K	Cr-K	Fe-L	Co-L	Ni-L
Pt1	15.21	5.20	4.78	0.28	3.75	28.10	17.42	14.70	10.56
Pt2	16.04	1.06	5.28	0.75	6.25	21.00	20.32	13.01	16.29
Pt3	7.30	2.52	5.72	1.90	8.56	16.34	21.62	14.91	21.13
Pt4	2.85	12.20	2.65	0.25	3.52	16.28	25.22	14.48	22.55

Fig. 2. SEM views and EDS analysis of the sample subjected to 2 h sintering process at 1200 °C in Ar environment and borided for 2 h at a) 900 °C, b) 1000 °C, c) 1100 °C.

with densities closer to 100% theoretical with P/M by using different additives, by increasing the cold compaction pressure, or by using other sintering techniques (e.g. liquid phase sintering).

XRD analyses of the borided samples after being produced by P/M method is given in Fig. 3. After sintering, FCC (FeNi) (JCPDS#00-047-1405), BCC (FeCr/AlNi) (JCPDS#01-77-7598) and Sigma (JCPDS#01-081-4950) phases were identified in the sample. In high entropy alloys, one or more phases can be seen depending on the alloying elements and their interactions [37]. It can be said that the effect of sigma phase on the hardness of the alloy was particularly high. After boriding, various metal boride phases were formed instead of these phases. Ni_2B (JCPDS#01-074-5462), Co_2B (JCPDS#01-075-1063), Cr_5B_3 (JCPDS#00-031-0396), Fe_2B (JCPDS#00-036-1332), TiB_2 (JCPDS#01-078-3430), CrB (JCPDS#01-081-3392) and AlB_{12} (JCPDS#00-012-0639) phases were determined in the borided sample at 900 °C for 2 h. With increasing the boriding temperature to 1000 °C, NiB (JCPDS#01-074-1207), Co_2B (JCPDS#01-075-1063), Fe_2B (JCPDS#00-036-1332), TiB_2 (JCPDS#01-078-3430), CrB (JCPDS#01-081-3392), Cr_5B_3 (JCPDS#00-031-0396) phases have been identified. In the sample borided at 1100 °C, NiB (JCPDS#01-074-1207), Ni_2B (JCPDS#01-074-5462), CrB (JCPDS#01-081-3392), Co_2B (JCPDS#01-075-1063), TiB_2 (JCPDS#01-078-3430), AlB_{12} (JCPDS#00-012-0639), Fe_2B (JCPDS#00-036-1332) and Fe_3B (JCPDS#00-062-0387) phases were found.

3.3. Mechanical properties

Microhardness, nanoindentation tests and layer thickness results are given in Table 3. The borided samples have a coating of 255–363 µm in thickness. Depending on the boriding temperature, the thickness of the boride layer changes from 253 µm at 900 °C, to 302 µm at 1000 °C, to 363 µm at 1100 °C. Diffusion increased with increasing temperature and accordingly, the thickness of the boride layer increased [38]. It has been reported in the literature that thicker coating layers are obtained with lower activation energy values [17,39,40]. Obtaining boride layers with greater thickness compared to those obtained in wrought materials [27] can be counted as an advantage for the P/M alloy. Porosity and grain boundaries in P/M materials can serve as pathways for the diffusion of boron.

While the hardness value of the sintered sample was 531 H V, the hardness values of the sintered + borided samples increased approximately 3 times and reached an average range of 1461–1646 H V. The improved hardness achieved in borided HEAs is a result of the formation of hard borides in the boride layer as well as solid solution strengthening in the HEA substrate [38] due to the diffusion of boron. Complex metal borides (M_xB_y) which formed on the surface of HEAs provided an increase in surface hardness. The obtained boride layers on powder metallurgy HEAs have lower hardness values compared to boride layers obtained in borided wrought HEAs (1442–1957 H V) [27] and this because of oxides and porosity inherent to P/M materials. Similarly, the lower hardness of the boride layers formed on the surface of P/M steels compared to those formed on wrought steels (1650–2300 H V) is related to their porosity and oxide content.

There was some increase in the hardness values of the boride layers with increasing boriding temperature. This situation can be attributed to the decrease in the formation of oxides with the increase of the boriding temperature. The microhardness profiles of the samples (from surface to the interior) are given in Fig. 4. While it has been stated in many studies that the hardness values obtained on the steels decrease from the surface to interior, in borided $CoCrFeNiAl_{0.25}Ti_{0.5}$ alloy the highest hardness values were obtained in the homogeneous portion of the coating underneath the rough surface (Fig. 2). It is possible to link this to the high concentration of oxides.

From hardness measurements made with nano-indentation, it was determined that the nanohardness values of the sample sintered in Ar medium was 6.23 GPa, whereas it was in the range of 15.00–17.72 GPa in borided samples. Significant differences were observed in the micro and nanoscale values of the samples. There are several reasons for this. Firstly, microhardness gives the average hardness value of the region tested, while nanohardness gives the hardness value taken over a smaller area of the material. Secondly, a load is applied to a very small part of

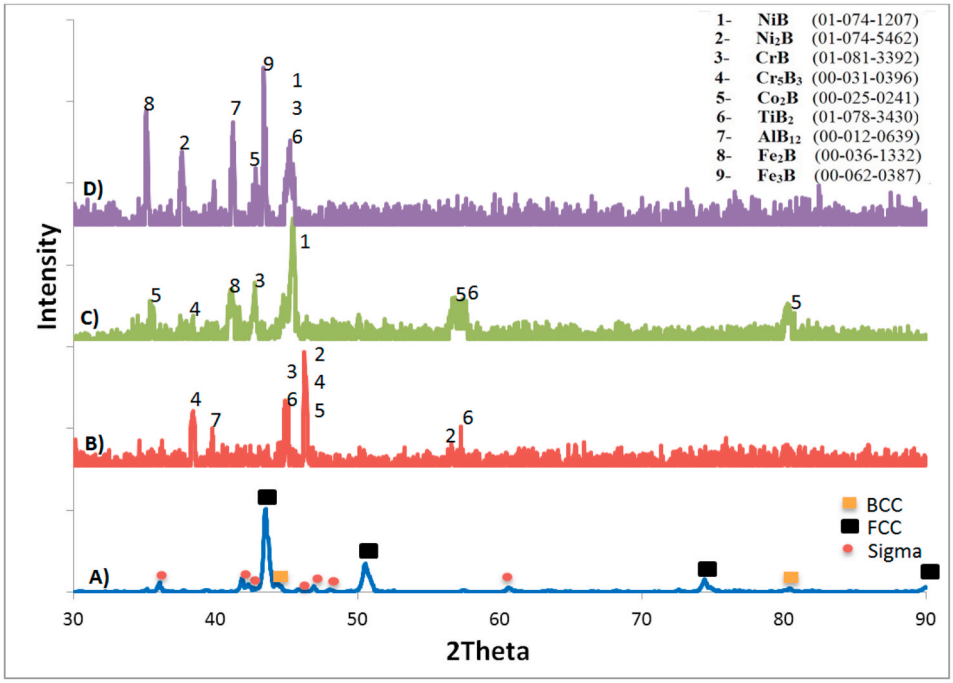

Fig. 3. XRD analysis obtained after sintering and boriding operations of $CoCrFeNiAl_{0.25}Ti_{0.5}$ alloy: a) Sintered at 1200 °C, b) Borided at 900 °C, c) Borided at 1000 °C, d) Borided at 1100 °C.

Table 3
Microhardness, nanoindentation test and layer thickness results for the sintered and borided $CoCrFeNiAl_{0.25}Ti_{0.5}$ alloy.

Sample	Micro-hardness (Hv)	Boride layer thickness (μm)		Nanoindentation Tests	
			Fracture Toughness ($MPa.m^{1/2}$)	Average hardness (GPa)	Modulus of elasticity (GPa)
S1	531 (≈5.02 GPa)	–	–	6.23	47.07
S2	1461 (≈14.33 GPa)	255 ± 25	4.25	15.00	140.56
S3	1574 (≈15.44 GPa)	302 ± 18	4.02	15.67	140.77
S4	1646 (≈16.14 GPa)	363 ± 23	3.57	17.72	151.53

the material in nanoindentation. This is thought to allow higher and more accurate nanohardness values. Due to thermo-chemical treatment, there may be some residual stresses in the material. Hernandez et al. [41] stated that the nanohardness-depth profiling is depend on the residual stress generated during the coating growth and this have a serious effect on nanohardness values. For this reason, it should not be forgotten that residual stresses may also have an effect on hardness values. The nanoindentation hardness values are approximately 2–5% higher than the measured microhardness values. This is to be expected, since nanoindentation uses the projected contact area at peak load A_c instead of the residual projected area A_r and also assumes purely elastic contact in the indentation process [38]. Therefore, it is possible that nano hardness values are slightly higher than micro-hardness values, as stated in the literature [42]. Hardness values of 1452–1525 H V by Koç [36] and 1202–1705 H V by Erdogan et al. [35] were reported for different steels produced with P/M and subjected to borosintering. The results obtained in the present study are therefore compatible with the literature. After boriding, up to 3 times improvement was achieved in terms of both hardness and modulus of elasticity. This shows that boriding can improve certain mechanical properties of HEAs such as elastic modulus and hardness. In samples borided at 900, 1000 and 1100 °C, fracture toughness values were 4.25, 4.02 and 3.57 MPa $m^{1/2}$, respectively. Fracture toughness can play a serious role in an application [43]. The brittleness of the coating layers increased with increasing hardness. Certain morphological changes also occurred within the boride layers, which affected the mechanical properties. Increasing the boriding temperature also increased the hardness for this reason. Similarly, the increasing boriding temperature increased the thickness of the boride layer due to the ease of diffusion. It must be admitted that the overall increase in hardness makes plastic deformation difficult. The difficulty of plastic deformation, in other words, the decrease in the ability to shape change, also reduces fracture toughness. At this point, it is possible to say that the main factor that affects the brittleness is not the thickness of the boride but phase change. For example, the phases that occur in borided steels significantly affect fracture toughness. The hardness of the boride layer significantly affects its fracture toughness. The fracture toughness values of the harder FeB layer obtained in steel is lower, while the relatively softer Fe_2B layer has higher fracture toughness [43–45]. The fracture toughness values obtained in this study are higher than FeB and closer to values observed for Fe_2B. It is known that surfaces are desired to be as hard as possible for certain applications such as wear. However, the increase in hardness generally decreases fracture toughness. At this point, it is necessary to look at the application point. If working under low loads, high hardness low fracture toughness will not be a problem. However, if high loads are in question, high fracture toughness will be beneficial. The use of a silicon-free boriding agent is thought to have had a positive effect on fracture toughness. Nickel silicide phases which occur during the boriding with silicon-containing Ekabor II powders have been found to generally reduce the fracture toughness [28–30]. The absence of silicon in the boriding agent and the substrate eliminated such a possibility.

According to the results of nano-indentation, the elastic moduli of the sintered + borided samples was in the range of 140–150 GPa while it was found to be around 47 GPa in the sample sintered in Ar. Therefore, it can be said that the boriding process has an important effect on

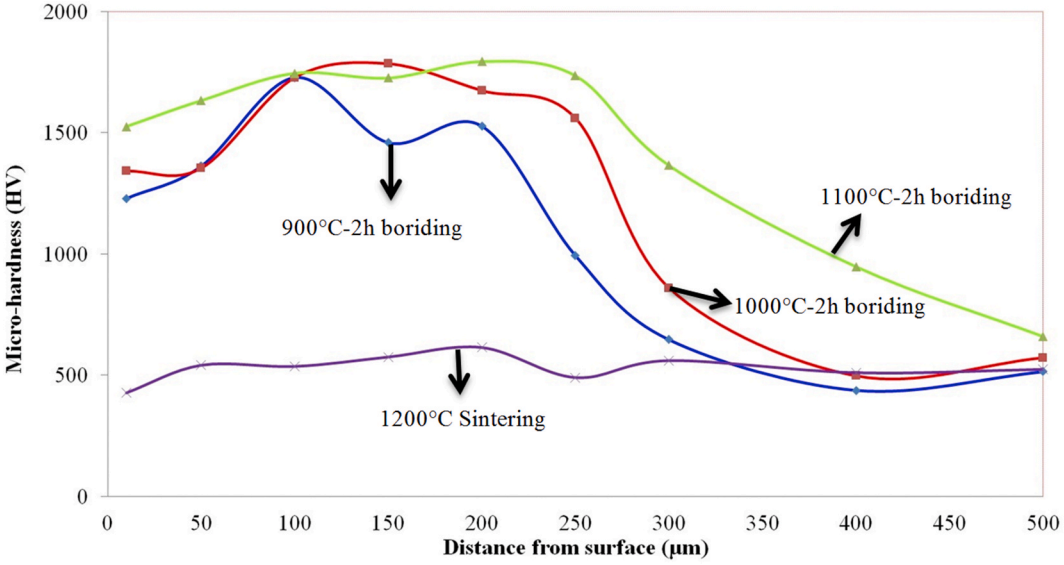

Fig. 4. Microhardness distribution of the samples from surface to the inner regions.

improving the modulus of elasticity. The new phases formed due to the boriding process caused changes in the elastic modulus values. This situation can be attributed to the strong new boride bonds which were formed after the boriding process. Boride phases are known to have a high elastic modulus [46]. In addition, there was a slight increase in the modulus of elasticity with increasing boriding temperature. However, in the literature, it is stated that the elastic moduli of boride layers (FeB, Fe_2B, CrB, NiB etc.) are in the range of 200–350 GPa [45,47,48]. The reason for the lower modulus of elasticity values obtained in the study can be attributed to the production of samples by powder metallurgy. The presence of porosity and oxide islets in the boride layer had a negative effect on the modulus of elasticity.

4. Conclusion

In this study, a high entropy $CoCrFeNiAl_{0.25}Ti_{0.5}$ alloy was sintered at 1200 °C for 2 h and subsequently subjected to boriding treatments. Boriding process was carried out for 2 h at 900, 1000 and 1000 °C using a 90 wt% B_4C + 10 wt% KBF_4 powder mixture. The microstructures, hardnesses, densities, surface roughness and nanoindentation properties of samples were investigated. Boriding of the HEAs was carried out successfully and improvements in surface properties were observed. The results obtained are briefly summarized below:

- With the density values ranging from 6.35 to 6.72 gr/cm^3, relative density values ranging from 85% to 90% were obtained. Surface roughness values increased with the boriding process but decreased with the boriding temperature.
- While FCC, BCC and sigma phases were observed after sintering, various metal borides were formed on the surface after the boriding process. After the boriding process, the elements in the alloy combined with the boron to form various boride phases. The boride layer was morphologically continuous and devoid of microcracks.
- Depending on the boriding temperature, 255 to 363 µm-thick coatings were obtained. With increasing boriding temperature, layer thickness and hardness increased. Owing to the formation of hard boride phases, the microhardness values, which were 531 H V after sintering, increased to 1461–1646 H V by boriding.
- The fracture toughness values of the boride layer were between 3.57 and 4.25 MPa m$^{1/2}$ in agreement with fracture toughness values of the boride phases previously reported in the literature.
- Modulus of elasticity values in the range of 140–151 GPa were found to be slightly lower than the values obtained in wrought materials reported in the literature. The relatively low modulus of elasticity in the boride coating was attributed to the existence of porosity and oxides in the structure.

Declaration of competing interest

The authors declare that they have no known competing financial interests or personal relationships that could have appeared to influence the work reported in this paper.

References

[1] A. Erdoğan, M.S. Gök, S. Zeytin, Analysis of the high-temperature dry sliding behavior of CoCrFeNiTi0.5Alx high-entropy alloys, Friction 8 (1) (2020) 198–207, https://doi.org/10.1007/s40544-019-0278-2.
[2] N.D. Stepanov, D.G. Shaysultanov, G.A. Salishchev, M.A. Tikhonovsky, Structure and mechanical properties of a light-weight AlNbTiV high entropy alloy, Mater. Lett. 142 (2015) 153–155, https://doi.org/10.1016/j.matlet.2014.11.162.
[3] A. Erdogan, T. Yener, S. Zeytin, Fast production of high entropy alloys (CoCrFeNiAlxTiy) by electric current activated sintering system, Vacuum 155 (2018) 64–72, https://doi.org/10.1016/j.vacuum.2018.05.027.
[4] N. Nayan, G. Singh, S.V.S.N. Murty, A.K. Jha, B. Pant, K.M. George, U. Ramamurty, Hot deformation behaviour and microstructure control in AlCrCuNiFeCo high entropy alloy, Intermetallics 55 (2014) 145–153, https://doi.org/10.1016/j.intermet.2014.07.019.
[5] Z. Fu, W. Chen, Z. Chen, H. Wen, E.J. Lavernia, Influence of Ti addition and sintering method on microstructure and mechanical behavior of a medium-entropy Al0.6CoNiFe alloy, Mater. Sci. Eng. 619 (2014) 137–145, https://doi.org/10.1016/j.msea.2014.09.077.
[6] A. Erdogan, K.M. Doleker, S. Zeytin, Effect of Al and Ti on high-temperature oxidation behavior of CoCrFeNi-based high-entropy alloys, J. Occup. Med. 71 (2019) 3499–3510, https://doi.org/10.1007/s11837-019-03679-2.
[7] Y. Yu, J. Wang, J. Li, H. Kou, W. Liu, Characterization of BCC phases in AlCoCrFeNiTixhigh entropy alloys, Mater. Lett. 138 (2015) 78–80, https://doi.org/10.1016/j.matlet.2014.09.100.
[8] U. Çavdar, B.S. Ünlü, A.M. Pinar, E. Atik, Mechanical properties of heat treated iron based compacts, Mater. Des. 65 (2015) 312–317, https://doi.org/10.1016/j.matdes.2014.09.015.
[9] T. Yener, S.C. Yener, S. Zeytin, Nb addition effect on microstructural properties of Ti–TiAl3 in situ composites produced by resistive sintering, J. Therm. Anal. Calorim. 134 (2018) 1359–1365, https://doi.org/10.1007/s10973-018-7636-6.
[10] M. Ali, F. Ahmad, P. Sri, N. Yahya, M. Aslam, Investigation of boron effect on the densification of Fe-50 % Ni soft magnetic alloys produced by powder metallurgy route, Mater. Today Proc. 16 (2019) 2210–2218, https://doi.org/10.1016/j.matpr.2019.06.112.
[11] H. Kulkarni, V.V. Dabhade, Green machining of powder-metallurgy-steels (PMS): an overview, J. Manuf. Process. 44 (2019) 1–18, https://doi.org/10.1016/j.jmapro.2019.05.009.

[12] J.M.C. Azevedo, A. CabreraSerrenho, J.M. Allwood, Energy and material efficiency of steel powder metallurgy, Powder Technol. 328 (2018) 329–336, https://doi.org/10.1016/j.powtec.2018.01.009.
[13] R. Neystani, B. Beidokhti, M. Amelzadeh, Fabrication of dissimilar Fe-Cu-C powder metallurgy compact/steel joint using the optimized resistance spot welding, J. Manuf. Process. 43 (2019) 200–206, https://doi.org/10.1016/j.jmapro.2019.05.014.
[14] F.L. Serafini, M. Peruzzo, I. Krindges, M.F.C. Ordoñez, D. Rodrigues, R.M. Souza, M.C.M. Farias, Microstructure and mechanical behavior of 316L liquid phase sintered stainless steel with boron addition, Mater. Char. 152 (2019) 253–264, https://doi.org/10.1016/j.matchar.2019.04.009.
[15] M.W. Wu, W.Z. Cai, Z.J. Lin, S.H. Chang, Liquid phase sintering mechanism and densification behavior of boron-alloyed Fe-Ni-Mo-C-B powder metallurgy steel, Mater. Des. 133 (2017) 536–548, https://doi.org/10.1016/j.matdes.2017.08.011.
[16] T. Balusamy, T.S.N. Sankara Narayanan, K. Ravichandran, I. Song Park, M.H. Lee, Pack boronizing of AISI H11 tool steel: role of surface mechanical attrition treatment, Vacuum 97 (2013) 36–43, https://doi.org/10.1016/j.vacuum.2013.04.006.
[17] K. Genel, Boriding kinetics of H13 steel, Vacuum 80 (2006) 451–457, https://doi.org/10.1016/j.vacuum.2005.07.013.
[18] N. López-Perrusquia, J. Martínez-Trinidad, R. Escobar-Galindo, M. Ortiz-Domínguez, A. Meneses-Amador, I. Campos-Silva, Characterization of AISI 4140 borided steels, Appl. Surf. Sci. 256 (2009) 2372–2379, https://doi.org/10.1016/j.apsusc.2009.10.070.
[19] Y. Kayali, Investigation of diffusion kinetics of borided AISI P20 steel in microwave furnace, Vacuum 121 (2015) 129–134, https://doi.org/10.1016/j.vacuum.2015.08.006.
[20] S. Sahin, C. Meric, Investigation of the effect of boronizing on cast irons, Mater. Res. Bull. 37 (2002) 971–979, https://doi.org/10.1016/S0025-5408(02)00697-9.
[21] A. Erdogan, Boriding temperature effect on micro-abrasion wear resistance of borided tool steel, J. Tribol. 141 (2019), https://doi.org/10.1115/1.4044859.
[22] S. Taktak, Tribological behaviour of borided bearing steels at elevated temperatures, Surf. Coating. Technol. 201 (2006) 2230–2239, https://doi.org/10.1016/j.surfcoat.2006.03.032.
[23] T. Balusamy, T.S.N. Sankara Narayanan, K. Ravichandran, I.S. Park, M.H. Lee, Effect of surface mechanical attrition treatment (SMAT) on pack boronizing of AISI 304 stainless steel, Surf. Coating. Technol. 232 (2013) 60–67, https://doi.org/10.1016/j.surfcoat.2013.04.053.
[24] M. Sabri Gok, A. Erdogan, M. Öge, A. Günen, Dry sliding wear behavior of borided hot-work tool steel at elevated temperatures, Surf. Coating. Technol. 328 (2017) 54–62, https://doi.org/10.1016/j.surfcoat.2017.08.008.
[25] L. Hou, J. Hui, Y. Yao, J. Chen, J. Liu, Effects of boron content on microstructure and mechanical properties of AlFeCoNiBx high entropy alloy prepared by vacuum arc melting, Vacuum 164 (2019) 212–218, https://doi.org/10.1016/j.vacuum.2019.03.019.
[26] F. Chang, B. Cai, C. Zhang, B. Huang, S. Li, P. Dai, Thermal stability and oxidation resistance of FeCr x CoNiB high-entropy alloys coatings by laser cladding, Surf. Coating. Technol. 359 (2019) 132–140, https://doi.org/10.1016/j.surfcoat.2018.12.072.
[27] T. Lindner, M. Löbel, B. Sattler, T. Lampke, Surface hardening of FCC phase high-entropy alloy system by powder-pack boriding, Surf. Coating. Technol. 371 (2019) 389–394, https://doi.org/10.1016/j.surfcoat.2018.10.017.
[28] A. Gunen, E. Kanca, Microstructure and mechanical properties of borided inconel 625 superalloy, Materia 22 (2) (2017), https://doi.org/10.1590/s1517-707620170002.0161.
[29] D. Mu, B. Shen, C. Yang, X. Zhao, Microstructure analysis of boronized pure nickel using boronizing powders with SiC as diluent, Vaccum 83 (2009) 1481–1484, https://doi.org/10.1016/j.vacuum.2009.06.048.
[30] I. Ozbeka, H. Akbulut, S. Zeytin, C. Bindal, A.H. Ucisikb, The characterization of borided 99 . 5 % purity nickel. https://doi.org/10.1016/S0257-8972(99)00667-2, 2000, 126, 166-170.
[31] D.C. Lou, O.M. Akselsen, J.K. Solberg, M.I. Onsoien, J. Berget, N. Dahl, Silicon-boronising of nimonic 90 superalloy. https://doi.org/10.1016/j.surfcoat.2005.03.030, 2006, 200, 3582-3589.
[32] W.C. Oliver, Measurement of Hardness and Elastic Modulus by Instrumented Indentation : Advances in Understanding and Refinements to Methodology, 2004.
[33] L.G. Yu, K.A. Khor, G. Sundararajan, Boride layer growth kinetics during boriding of molybdenum by the Spark Plasma Sintering, SPS) technology 201 (2006) 2849–2853, https://doi.org/10.1016/j.surfcoat.2006.05.042.
[34] J. Karwan-Baczewska, The properties of Fe-Ni-Mo-Cu-B materials produced via liquid phase sintering, Arch. Metall. Mater. 56 (2011) 789–796, https://doi.org/10.2478/v10172-011-0087-8.
[35] A. Erdogan, B. Kursuncu, A. Günen, M. Kalkandelen, M.S. Gok, A new approach to sintering and boriding of steels " Boro-sintering " : formation , microstructure and wear behaviors, Surf. Coating. Technol. 386 (2020) 125482, https://doi.org/10.1016/j.surfcoat.2020.125482.
[36] V. Koç, Effect of boro-sintering process on mechanical properties and wear behaviour of low alloy steel produced by powder metallurgy Effect of boro-sintering process on mechanical properties and wear behaviour of low alloy steel produced by powder metallurgy, Mater. Res. Express 6 (2019) 1265c3, https://doi.org/10.1088/2053-1591/ab636b.
[37] A. Erdogan, K. Mert, S. Zeytin, Effect of laser re-melting on electric current assistive sintered CoCrFeNiAl x Ti y high entropy alloys : formation , micro-hardness and wear behaviors, Surf. Coating. Technol. 399 (2020) 126179, https://doi.org/10.1016/j.surfcoat.2020.126179.
[38] J. Hou, M. Zhang, H. Yang, J. Qiao, Y. Wu, Surface strengthening in Al0.25CoCrFeNi high-entropy alloy by boronizing, Mater. Lett. 238 (2019) 258–260, https://doi.org/10.1016/j.matlet.2018.12.029.
[39] Y. Kayali, Diffusion kinetics of borided AISI 52100 and AISI 440C steels. https://doi.org/10.1016/j.vacuum.2012.03.030, 2012, 86.
[40] I. Uslu, H. Comert, M. Ipek, O. Ozdemir, C. Bindal, Evaluation of borides formed on AISI P20 steel. https://doi.org/10.1016/j.matdes.2005.06.013, 2007, 28, 55-61.
[41] L.C. Herná, L. Ponce, A. Fundora, E. Ló, Nanohardness and residual stress in TiN coatings. https://doi.org/10.3390/ma4050929, 2011, 929-940.
[42] L. Qian, M. Li, Z. Zhou, H. Yang, X. Shi, Comparison of nano-indentation hardness to microhardness 195 (2005) 264–271, https://doi.org/10.1016/j.surfcoat.2004.07.108.
[43] A. Erdoğan, Investigation of high temperature dry sliding behavior of borided H13 hot work tool steel with nanoboron powder, Surf. Coating. Technol. 357 (2019) 886–895, https://doi.org/10.1016/j.surfcoat.2018.10.066.
[44] U. Sen, Fracture toughness of borides formed on boronized ductile iron 26 (2005) 175–179, https://doi.org/10.1016/j.matdes.2004.05.015.
[45] M. Kulka, N. Makuch, A. Piasecki, Nanomechanical characterization and fracture toughness of FeB and Fe 2 B iron borides produced by gas boriding of Armco iron, Surf. Coating. Technol. 325 (2017) 515–532, https://doi.org/10.1016/j.surfcoat.2017.07.020.
[46] M.M.E. Ali, J. Chen, I. Harran, B. Sun, X. Cai, H. Wang, L. Tao, Y. Chen, The pressure-induced chemical structures and properties trend for compressed iron-boride compounds, J. Phys. Chem. Solid. 127 (2019) 238–244, https://doi.org/10.1016/j.jpcs.2018.12.028.
[47] I. Campos-silva, M. Flores-jiménez, G. Rodríguez-castro, E. Hernández-sánchez, Improved fracture toughness of boride coating developed with a diffusion annealing process, Surf. Coating. Technol. 237 (2013) 429–439, https://doi.org/10.1016/j.surfcoat.2013.05.050.
[48] M.S. Meruvia, P. César, S. Júnior, R.D. Torres, Tribocorrosion behavior of boronized AISI 4140 steel 352 (2018) 265–272, https://doi.org/10.1016/j.surfcoat.2018.07.101.